Macroscopic electromagnetic response of arbitrarily shaped spatially dispersive bodies formed by metallic wires

João T. Costa and Mário G. Silveirinha*

University of Coimbra, Electrical Engineering Department–Instituto de Telecomunicações, 3030-290 Coimbra, Portugal

(Received 8 May 2012; revised manuscript received 6 July 2012; published 17 August 2012)

In media with strong spatial dispersion, the electric displacement vector and the electric field are typically linked by a partial differential equation in the bulk region. The objective of this work is to highlight that in the vicinity of an interface, the relation between the macroscopic fields cannot be univocally determined from the bulk response of the involved materials but instead requires knowledge of internal degrees of freedom of the materials. We derive such a relation for the particular case of "wire media" and describe a numerical formalism that enables characterization of the electromagnetic response of arbitrarily shaped spatially dispersive bodies formed by arrays of crossed wires. The possibility of concentrating the electromagnetic field in a narrow spot by tapering a metamaterial waveguide is discussed.

DOI: 10.1103/PhysRevB.86.075129 PACS number(s): 42.70.Qs, 78.20.Ci, 41.20.Jb

I. INTRODUCTION

Spatially dispersive materials have the peculiar property that the macroscopic polarization vector depends not only on the macroscopic electric field but also on its spatial derivatives.[1] As is well known, this implies that the electric displacement vector $\mathbf{D}$ is related to the electric field $\mathbf{E}$ through a constitutive relation of the form $\mathbf{D} = \bar{\bar{\varepsilon}}(\omega, -i\nabla) \cdot \mathbf{E}$, which for the case of fields with a plane wave-type spatial dependence of the form $e^{i\mathbf{k}\cdot\mathbf{r}}$ reduces simply to $\mathbf{D} = \bar{\bar{\varepsilon}}(\omega,\mathbf{k}) \cdot \mathbf{E}$. The dielectric function $\bar{\bar{\varepsilon}}(\omega,\mathbf{k})$ fully characterizes the electromagnetic response of the material in the bulk region for any macroscopic excitation. However, any realistic physical system is necessarily of finite extent, and some of the most interesting electromagnetic phenomena—such as the refraction and reflection of light, field localization, and waveguiding—have their origin in interface effects. In general, the constitutive relation $\mathbf{D} = \bar{\bar{\varepsilon}}(\omega, -i\nabla) \cdot \mathbf{E}$ does not hold exactly at the boundary, and this can create ambiguities in the solution of electromagnetic problems involving bodies formed by spatially dispersive materials.

To illustrate this, let us consider the simple case in which both the electric field and the electric displacement field are oriented in the z-direction and are linked in the bulk region as follows:

$$D_z = \varepsilon(\omega, -i\nabla) E_z. \tag{1}$$

Furthermore, for the purpose of illustration, it is assumed that the material is nonmagnetic and that the dielectric function is a rational function of the wave vector so that

$$\varepsilon(\omega,\mathbf{k}) = \varepsilon_h + \frac{b_0}{a_0 - a_2 k_x^2 + \cdots}, \tag{2}$$

where ε_h, b_0, a_0, a_2, ..., are independent of the wave vector but in general may depend on frequency. It is supposed that the material has a center of symmetry at the microscopic level so that the dielectric function is an even function of $\mathbf{k}$. Moreover, it is assumed without loss of generality that $\varepsilon(\omega,\mathbf{k})$ depends exclusively on $k_x \leftrightarrow -i\frac{\partial}{\partial x}$. Clearly, if the only nonzero coefficients are a_0 and a_2, the D_z and E_z fields satisfy the following partial differential equation in the bulk region:

$$a_0 P_{c,z} + \partial_x^2 (a_2 P_{c,z}) = b_0 E_z, \tag{3}$$

where we defined $P_{c,z} = D_z - \varepsilon_h E_z$, which may be regarded as the polarization of the medium with respect to a background with permittivity ε_h. For a material with a local response, the coefficient a_2 vanishes.

Let us now suppose that the plane $x = 0$ corresponds to an interface between two different materials, in which one of the materials occupies the semispace $x > 0$, whereas the second material occupies the region $x < 0$, and that the constitutive relation in both bulk materials is of the generic form of Eq. (2). Evidently, the coefficients a_0, a_2, and b_0 in general differ in the two materials. Therefore, it is tempting to consider that the $P_{c,z}$ and E_z fields are related in all space by

$$a_0(x) P_{c,z} + \partial_x^2 (a_2(x) P_{c,z}) = b_0(x) E_z. \tag{4}$$

This equation, together with the standard macroscopic Maxwell equations $\nabla \times \mathbf{E} = i\omega\mu_0 \mathbf{H}$ and $\nabla \times \mathbf{H} = \mathbf{j}_{\text{ext}} - i\omega\mathbf{D}$ and the Sommerfeld radiation conditions, determines, for a given excitation $\mathbf{j}_{\text{ext}}$, the electromagnetic fields $(\mathbf{E},\mathbf{H})$ in all space. The outlined ideas and other variants are the basis of several studies that aim to characterize the electromagnetic response of either nanoparticles or macroscopic bodies made of natural media or metamaterials with spatial dispersion.[2–10] The main objective of the present study is to demonstrate with specific examples that even though in some scenarios this direct approach captures correctly the physical response of a system, in other cases it may produce inaccurate results.

Indeed, even if the bulk constitutive relation in Eq. (3) holds exactly up to the boundary, in general the form of Eq. (4) remains unjustified at $x = 0$, i.e., at the boundary. The reason is that there are many inequivalent ways of relating $P_{c,z}$ and E_z through a differential equation, but these reduce to Eq. (3) in the bulk regions. For an abrupt interface, the coefficients a_0, a_2, and b_0 are discontinuous at $x = 0$; therefore, *a priori* nothing forbids $P_{c,z}$ and E_z to be linked by, for example,

$$a_0(x) P_{c,z} + \partial_x [a_2(x) \partial_x P_{c,z}] = b_0(x) E_z \tag{5}$$

rather than by Eq. (4). The preceding equation is equivalent to Eq. (4) in the bulk regions (i.e., for $x \neq 0$, where

$a_2(x) = \text{const.}$) but not at $x = 0$. In fact, the form of Eq. (4) suggests that $\partial_x(a_2 P_{c,z})$ is continuous at the interface, whereas Eq. (5) implies that $a_2 \partial_x P_{c,z}$ is continuous at the interface. Hence, the two formulations imply different boundary conditions at the interfaces, even though they are equivalent in the bulk regions. In this discussion, it is implicit that the pertinent solution ($P_{c,z}$) is defined in a space of generalized functions and that the equations hold in the distributional sense.

Generally, when electromagnetic waves illuminate spatially dispersive bodies, "additional waves" can be excited; therefore, the classical boundary conditions that impose the continuity of the tangent fields at the interfaces are insufficient to solve a scattering problem based on mode matching. The usual way to fix this problem is to impose additional boundary conditions (ABCs).[1,11–13] However, in a framework where the bulk constitutive relations are extended across the interface [e.g., Eqs. (4) or (5)], the scattering problem is complete and logically consistent on its own; hence, it does not require further boundary conditions to be explicitly imposed. However, as should be clear from the preceding argument, the structure of the adopted constitutive relation [e.g., Eqs. (4) or (5)] at the boundary may indirectly enforce an ABC at an interface at which the coefficients of the equation are discontinuous. Therefore, knowledge of the correct form of the constitutive relation across the interface is intimately related to knowledge of ABCs, and these are complementary aspects of the same problem.

The previous discussion illustrates that there are distinct ways of linking $P_{c,z}$ and E_z close to the boundary that are consistent with constitutive relations in the bulk regions. Indeed, there are infinitely many possibilities of linking $P_{c,z}$ and E_z at the boundary, and some of them cannot even be formulated in terms of the coefficients a_0, a_2, and b_0 of the effective medium model. For example, if we replace the term $\partial_x^2(a_2 P_{c,z})$ in Eq. (4) by the term $A(x)\partial_x[A^{-1}(x)\partial_x(a_2 P_{c,z})]$ where $A(x)$ is an *arbitrary* piecewise constant function of x discontinuous at $x = 0$, we obtain other inequivalent ways of linking $P_{c,z}$ and E_z in all space involving an extra parameter ($A(x)$), which is unrelated to the bulk material dielectric function.

In this work, our aims are (1) to highlight that the correct manner of extending the bulk constitutive relations across the interface requires knowledge of internal (microscopic) degrees of freedom of the involved materials at the boundary, and (2) to discuss how the Maxwell equations can be solved using numerical methods in the presence of arbitrarily shaped bodies with a spatially dispersive response. To this end, we investigate the electromagnetic response of arbitrarily shaped bodies of "wire media," which are metamaterials known to have a strongly spatially dispersive response[14–17] and interesting applications in the emerging fields of nanophotonics and plasmonics.[18–26]

The uniaxial wire medium[14] is the most well-known metamaterial with a nonlocal response, but such a property is also inherent to other wire media topologies, such as arrays of long helices and arrays of both connected and nonconnected wires.[13,17] In this work, we choose the double wire medium—a double array of nonconnected metallic wires—for illustration purposes, but the theory can be trivially extended to other wire medium topologies. Based on an effective medium framework wherein the metamaterial response is expressed in terms of additional variables with known physical meaning,[27] we prove that the correct manner of linking the **D** and **E** fields across the boundary does not reduce to a simple Fourier inversion of the bulk constitutive relations, as in Eq. (4). We use our theory to develop a spatially dispersive finite-difference frequency-domain (FDFD-SD) numerical method that enables us to solve the Maxwell equations in scenarios wherein electromagnetic waves can interact with arbitrarily shaped bodies formed by wire media. We demonstrate with numerical simulations that if the host medium of the metallic wires is a dielectric, or even more drastically if the nanowires are in contact with a metallic surface, a numerical solution based on Eq. (4) may fail at the interfaces. We apply the FDFD-SD formalism to investigate applications of the double wire medium in superlensing[18] and in ultraconfined waveguiding. In this work, a time variation of the form $e^{-i\omega t}$ is assumed.

II. MODEL BASED ON THE BULK ELECTROMAGNETIC RESPONSE

The double wire medium is formed by two arrays of metallic wires with radius r_w such that each array of parallel wires is arranged in a square lattice with lattice constant a and tilted by $\pm 45^\circ$ with respect to the interfaces. One set of wires is oriented in the direction $\hat{\mathbf{u}}_1 = (1,0,1)/\sqrt{2}$, while the complementary set of wires is oriented in the direction $\hat{\mathbf{u}}_2 = (-1,0,1)/\sqrt{2}$. Both sets of wires lie in planes parallel to the *xoz* plane, and the distance between adjacent perpendicular wires is $a/2$ [Figs. 1(a) and 1(b)].

The wires stand in a host material with relative permittivity ε_h. The effective response of the double wire medium is characterized by a dielectric function $\bar{\bar{\varepsilon}}(\omega,\mathbf{k})$ such that[12,16,28]

$$\frac{\bar{\bar{\varepsilon}}}{\varepsilon_0} = \varepsilon_h \hat{\mathbf{u}}_y \hat{\mathbf{u}}_y + \varepsilon_{11} \hat{\mathbf{u}}_1 \hat{\mathbf{u}}_1 + \varepsilon_{22} \hat{\mathbf{u}}_2 \hat{\mathbf{u}}_2$$

$$\varepsilon_{ii}(\omega,k_i) = \varepsilon_h \left(1 + \frac{1}{\frac{1}{(\varepsilon_m/\varepsilon_h - 1) f_V} - \frac{\varepsilon_h(\omega/c)^2 - k_i^2}{\beta_p^2}} \right), \quad (6)$$

where $\varepsilon_0\varepsilon_m$ is the permittivity of the metal, $f_V = \pi(r_w/a)^2$ is the volume fraction of each set of wires, $\beta_p = \{2\pi/[\ln(a/2\pi r_w) + 0.5275]\}^{1/2}/a$ is the plasma wave number, and c is the speed of light in vacuum. For simplicity, in this work, we restrict our attention to the case of propagation along the *xoy* plane with $k_z = 0$ (or equivalently, $\partial_z = 0$), and assume that the only nontrivial electromagnetic field components are E_z, D_z, H_x, and H_y. In this scenario, the dielectric function

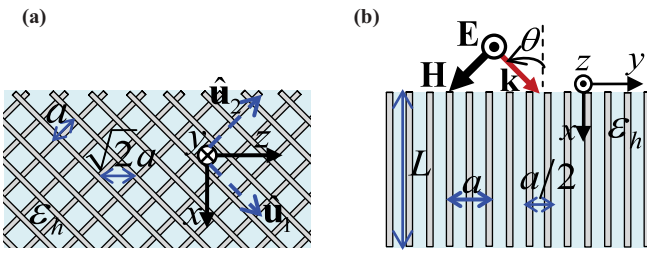

FIG. 1. (Color online) Cuts of a double wire medium along the (a) *xoy* and (b) *xoz* planes. The slab has thickness L.

reduces to a scalar in the xoy plane, $\varepsilon(\omega,k_x)=\varepsilon_{ii}(\omega,k_i)$, $i=1,2$, because for $k_z=0$, we have $k_1=k_x/\sqrt{2}=-k_2$. Therefore, in this situation, Eq. (6) becomes

$$\varepsilon(\omega,k_x)=\varepsilon_h\left(1+\frac{1}{\frac{1}{(\varepsilon_m/\varepsilon_h-1)f_V}-\frac{\varepsilon_h(\omega/c)^2-k_x^2/2}{\beta_p^2}}\right), \tag{7}$$

which is clearly of the same form as Eq. (2); i.e., it is a rational function of the wave vector.

Because the only non-zero-field components in the problems that we are interested in are E_z, D_z, H_x, and H_y, it is easily found that Maxwell equations $\nabla\times\mathbf{E}=i\omega\mu_0\mathbf{H}$ and $\nabla\times\mathbf{H}=\mathbf{j}_{\text{ext}}-i\omega\mathbf{D}$ reduce to the scalar equation

$$\frac{\partial^2}{\partial x^2}E_z+\frac{\partial^2}{\partial y^2}E_z+\left(\frac{\omega}{c}\right)^2\frac{D_z}{\varepsilon_0}=-i\omega\mu_0 j_{s,z}, \tag{8}$$

where $\mathbf{j}_{\text{ext}}=j_{s,z}\hat{\mathbf{z}}$ represents an external current density, i.e., an external excitation. Therefore, provided we are able to link E_z and D_z in all space, the Maxwell equations can be solved univocally. Next, we discuss how this can be done based on Eq. (7).

A. Constitutive relations in the bulk region

Similar to what was outlined in Sec. I, substituting Eq. (7) into Eq. (1) and calculating the inverse Fourier transform ($i\,k_x\leftrightarrow\partial_x$) of the resulting expression, it is possible to obtain a spatial relation between the electric field E_z and the electric displacement D_z that makes manifest the spatially dispersive nature of the response of the metamaterial:

$$\left[\frac{1}{2}\frac{\partial^2}{\partial x^2}+\varepsilon_h\left(\frac{\omega}{c}\right)^2+\beta_c^2\right]\frac{P_{c,z}}{\varepsilon_0}+\varepsilon_h\beta_p^2E_z=0, \tag{9}$$

where $\beta_c^2=-\frac{\beta_p^2}{(\varepsilon_m/\varepsilon_h-1)f_V}$ and $P_{c,z}=D_z-\varepsilon_0\varepsilon_hE_z$. This is analogous to Eq. (3) for the particular case of the double wire medium. $P_{c,z}$ is the contribution to the polarization vector due to the conduction currents in the nanowires. Thus, Eq. (9) effectively determines the response of the conduction polarization current to the "applied" macroscopic electric field.

A priori, Eq. (9) is only valid in the bulk region of the metamaterial. However, it can be trivially extended to scenarios wherein a metamaterial body is surrounded by a standard dielectric (e.g., air). Indeed, if we regard $\varepsilon_h\equiv\varepsilon_h(x,y)$ as a position-dependent function that represents the relative permittivity of the background dielectric regions, and similarly $\beta_p\equiv\beta_p(x,y)$ and $\beta_c\equiv\beta_c(x,y)$ as functions that vanish outside the metamaterial, it is clear that in a standard dielectric Eq. (9) reduces to

$$\left[\varepsilon_h\left(\frac{\omega}{c}\right)^2+\frac{1}{2}\frac{\partial^2}{\partial x^2}\right]P_{c,z}=0. \tag{10}$$

This relation is correct because in a standard dielectric $D_z=\varepsilon_0\varepsilon_hE_z$, or equivalently $P_{c,z}=0$. Thus, if we let $\varepsilon_h\equiv\varepsilon_h(x,y)$, $\beta_p\equiv\beta_p(x,y)$, and $\beta_c\equiv\beta_c(x,y)$ be space dependent, Eq. (9) yields the correct constitutive relations both in the bulk metamaterial and in the bulk dielectric region (i.e., in the region that surrounds the metamaterial body). If we assume that Eq. (9) also holds across the boundary—which as discussed in Sec. I in general may be a "leap of faith"—then it is possible to calculate the electromagnetic fields in all space by combining and solving Eqs. (8) and (9). In the next subsection, we briefly describe how this can be done numerically using the FDFD method.

B. FDFD discretization

The unknown fields (solution of Eqs. (8) and (9)) can be obtained using the well-known FDFD method based on Yee's mesh.[29] The discretization of the second-order derivatives in these equations is done based on the formulas proposed in Ref. 30

$$\frac{\partial^2}{\partial x^2}F(i,j)=\frac{F(i+1,j)-2F(i,j)+F(i-1,j)}{\Delta x^2} \tag{11a}$$

$$\frac{\partial^2}{\partial y^2}F(i,j)=\frac{F(i,j+1)-2F(i,j)+F(i,j-1)}{\Delta y^2}, \tag{11b}$$

where $F=P_{c,z}=D_z-\varepsilon_0\varepsilon_hE_z$; Δx and Δy are the grid spacing in the x- and y-directions, respectively; and the discrete indices (i,j) stand for a given ith and jth nodes of the grid mesh in the x- and y-directions, respectively. As discussed previously, $\varepsilon_h\equiv\varepsilon_h(x,y)$ is a position-dependent function that is equal to the host permittivity in the metamaterial, and equal to the permittivity constant in the dielectric material. However, $\beta_p\equiv\beta_p(x,y)$ and $\beta_c\equiv\beta_c(x,y)$ are set equal to zero outside the metamaterial.

We considered two FDFD solutions for the described problem. In the first approach, Eq. (9) is used in all regions of space to link E_z and D_z. We refer to this solution as the first direct inverse transform (DIT1) solution. In the second approach, we use Eq. (9) to link E_z and D_z inside the metamaterial, as well as for all nodes that are over the boundary. For nodes that are outside the metamaterial (such that all neighboring nodes are also outside the metamaterial), we use simply $D_z=\varepsilon_0\varepsilon_hE_z$ rather than Eq. (9). We refer to this implementation as the second direct inverse transform (DIT2) solution. The perfectly matched layer (PML) described in Ref. 31 is used to truncate the computation domain in both implementations.

III. MODEL BASED ON INTERNAL DEGREES OF FREEDOM OF THE MEDIUM

Recent works[13,27,32] have shown that the spatial dispersion inherent to wire media may be described by a quasistatic homogenization model that applies in a wide range of scenarios, including the case in which the wires are periodically loaded with conducting metallic bodies. In this homogenization framework, a current I and an additional potential φ are associated with each set of wires. The current may be identified with the current that flows along the metallic wires, whereas the additional potential is the average quasistatic potential drop from a given wire to the boundary of the respective unit cell (both the current and the additional potential are interpolated in a suitable manner so that they become continuous functions of the spatial coordinates).[27] As detailed in Appendix A, for the case of the double wire medium, the electrodynamics of the metamaterial is described by a 10-component state vector $\mathbf{F}=(\mathbf{E},\mathbf{H},\varphi_1,I_1,\varphi_2,I_2)$ that satisfies a differential system of

the form

$$\hat{\mathrm{L}} \cdot \mathbf{F} = +i\omega \hat{\mathrm{M}} \cdot \mathbf{F} + \mathbf{J}_{\mathrm{ext}}, \tag{12}$$

where $\hat{\mathrm{L}} = \hat{\mathrm{L}}(\nabla)$ is a linear differential operator, $\hat{\mathrm{M}} = \hat{\mathrm{M}}(\varepsilon_h, \mu_0, L_w, Z_w, C_w)$ is a material matrix that depends on the geometry of the array of metallic wires and on the electromagnetic properties of the involved materials, and $\mathbf{J}_{\mathrm{ext}}$ represents a source term.

This formalism based on the introduction of additional variables provides a framework within which the wire medium response is "local" (even though the electrodynamics is nonlocal) in the sense that the material response can be written in terms of the 10-component vector $\mathbf{F} = (\mathbf{E}, \mathbf{H}, \varphi_1, I_1, \varphi_2, I_2)$ through a linear operator ($\hat{\mathrm{M}}$) independent of the spatial derivatives. Hence, it is reasonable to assume that Eq. (12) holds even across a boundary between two regions with different structural parameters such that $\hat{\mathrm{M}} = \hat{\mathrm{M}}(x, y, z)$. Such premise is the basis of the ideas developed in this section, where we obtain a solution for the electromagnetic fields in all space relying on Eq. (12). A standard dielectric can also be described with this formalism, because it can be considered the limit of a nanowire material with vanishingly thin wires.

The effective medium formalism associated with Eq. (12) is based on knowledge of the dynamics of the additional variables I and φ, which have known physical meaning, and thus is based on knowledge of internal degrees of freedom (IDF) of the material.

A. Constitutive relations based on the internal degrees of freedom

In Appendix A, it is shown that in the general case where the structural parameters are arbitrary functions of the coordinates ($\hat{\mathrm{M}} = \hat{\mathrm{M}}(x, y, z)$), Eq. (12) reduces to

$$\frac{\varepsilon_h \beta_p^2}{2} \frac{\partial}{\partial x} \left[\frac{1}{\varepsilon_h \beta_p^2} \frac{\partial}{\partial x} \frac{P_{c,z}}{\varepsilon_0} \right] + \left[\varepsilon_h \left(\frac{\omega}{c} \right)^2 + \beta_c^2 \right] \frac{P_{c,z}}{\varepsilon_0} + \varepsilon_h \beta_p^2 E_z = 0, \tag{13a}$$

$$\frac{\partial^2}{\partial x^2} E_z + \frac{\partial^2}{\partial y^2} E_z + \left(\frac{\omega}{c} \right)^2 \frac{D_z}{\varepsilon_0} = -i\omega\mu_0 j_{s,z}. \tag{13b}$$

Evidently, Eq. (13b) is the same as Eq. (8). In addition, Eq. (13a) is the same as Eq. (9) in the bulk region, i.e., when β_p and ε_h are constant and independent of position. However, the two equations are different at the interfaces, because the parameters β_p, β_c, and ε_h may vary with space. This happens if, for example, either the permittivity of the host medium or the radii of the wires vary in space.

In the same manner as in Sec. II, here we assume that $\varepsilon_h = \varepsilon_h(x, y)$, $\beta_p = \beta_p(x, y)$, and $\beta_c = \beta_c(x, y)$. In a standard dielectric, we take the limit $\beta_p \to 0$ and put $\beta_c(x, y) = 0$. In this case, β_p cannot be chosen exactly equal to zero; otherwise, Eq. (13a) becomes singular.

B. FDFD discretization

The FDFD discretization of the system in Eqs. (13a) and (13b) is analogous to that already described in Sec. II B. The only relevant difference is that the second-order derivatives of Eqs. (13a) and (13b) are of the generic form $\frac{\partial}{\partial x} G(x, y) \frac{\partial}{\partial x} U(x, y)$, where $G(x, y) = 1/[\varepsilon_h(x, y)\beta_p^2(x, y)]$ and $U(x, y) = P_{c,z}/\varepsilon_0$. The derivative $\frac{\partial}{\partial x} G(x, y) \frac{\partial}{\partial x} U(x, y)$ is discretized in the following manner:

$$\left[\frac{\partial}{\partial x} G \frac{\partial}{\partial x} U \right](i, j) = \frac{A(i, j)U(i + 1, j)}{\Delta x^2} - \frac{B(i, j)U(i, j)}{\Delta x^2} + \frac{C(i, j)U(i - 1, j)}{\Delta x^2}, \tag{14}$$

where $A(i, j) = [G(i, j) + G(i + 1, j)]/2$, $B(i, j) = G(i, j) + [G(i + 1, j) + G(i - 1, j)]/2$ and $C(i, j) = [G(i, j) + G(i - 1, j)]/2$. The computation domain is truncated with a PML.[31] In this implementation, we use Eq. (13a) in all space (both in the metamaterial and in standard dielectrics or metals). We refer to this solution based on the internal degrees of freedom of the metamaterial as the IDF solution. The discretized equations for Eqs. (13a) and (13b) are given in Appendix B.

IV. NUMERICAL RESULTS AND DISCUSSION

Next, we compare the results obtained with the formulations of Secs. II and III and confirm that the form of constitutive relations at the interfaces is of crucial importance.

In the first example, we consider a double wire medium slab formed by perfect electric conductor (PEC) wires, i.e., $\varepsilon_m = -\infty$. The metamaterial has thickness L and is surrounded by air [Fig. 1(b)]. The permittivity of the host region in the double wire medium is taken as $\varepsilon_h = 10$, and the lattice constant a is such that $a = L/20$ and $r_w = 0.05a$. In Fig. 2, the reflection and transmission coefficients ρ and τ are depicted as functions of the normalized frequency $\omega L/c$ for a plane wave that illuminates the slab with an angle of incidence $\theta_i = 15^\circ$.

The green triangles and blue circles represent the results computed with FDFD-SD methods DIT1 and DIT2, respectively (see Sec. II B). These two approaches are based on Eq. (9). The orange stars were obtained using the FDFD-SD method IDF (see Sec. III B) based on knowledge of the internal structure of the metamaterial Eq. (13). In the DIT1 and IDF implementations, the parameter β_p^2 is taken as vanishingly small outside the metamaterial. Finally, the black solid curves in Fig. 2 were computed using an analytical approach derived in Ref. 12, based on mode matching and ABCs. It was demonstrated in Ref. 12 (and confirmed in Fig. 3) that this analytical method compares well with full-wave simulations that take into account all minute details of the microstructure of the metamaterial. Therefore, the solid curves can be regarded here as the *exact solution* of the problem.

Figure 2 shows that the DIT1 method can be quite inaccurate, as the green triangle curve for the amplitude of the transmission coefficient τ [Fig. 2(c)] largely mismatches the black solid curve obtained with the analytical model. This confirms that proper discretization of the electromagnetic fields at the interfaces between the spatially dispersive metamaterial and the air region is of crucial importance. However, the blue circle curves (DIT2) concur better with the analytical model. The results obtained with the IDF implementation (orange stars) yield near-perfect agreement with the analytical formalism. This supports that to model the electromagnetic response of spatially dispersive bodies correctly, it may be necessary to know some internal degrees of freedom of the metamaterial,

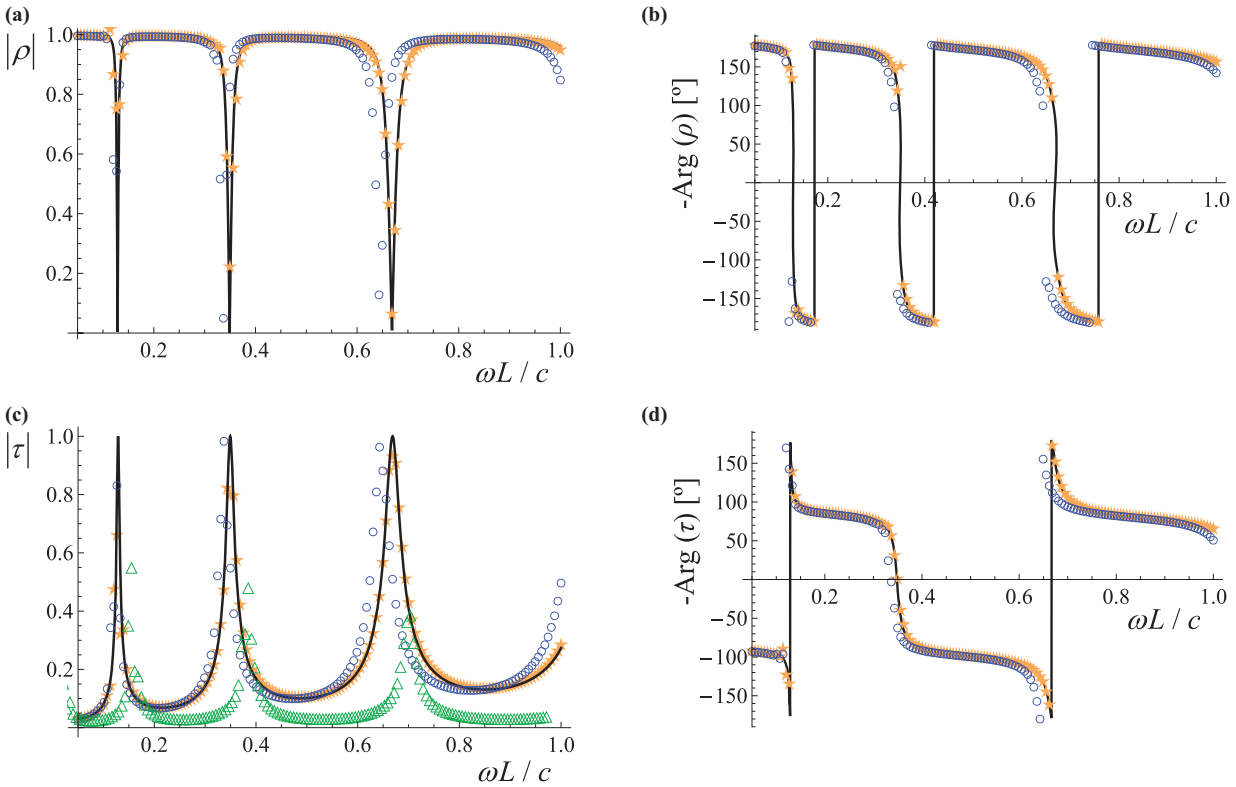

FIG. 2. (Color online) Reflection and transmission coefficients as functions of the normalized frequency for a double wire medium slab with thickness $L = 20a$ illuminated by a plane wave with the angle of incidence $\theta_i = 15°$. (a) Amplitude and (b) phase of the reflection coefficient ρ. (c) Amplitude and (d) phase of the transmission coefficient τ. Solid (black) curves indicate the mode-matching approach based on ABCs (Ref. 12). Stars (orange) indicate the IDF approach, triangles (green) indicate the DIT1 approach, and circles (blue) indicate the DIT2 approach (see Sec. II B).

which cannot be accessed simply from knowledge of the bulk electromagnetic response. In Fig. 3, we compare the results obtained with the IDF implementation and full-wave simulations[33] that take into account the microstructure of the metamaterial. As seen, the agreement is nearly perfect.

The several dips in the reflection characteristic in Fig. 2 are associated with Fabry-Pérot resonances. These resonances are ultra-subwavelength (e.g., the first dip of the reflection coefficient occurs at $\omega L/c \approx 0.13$, which corresponds to metallic wires with length $L_{wm} = \sqrt{2}L = 0.03\lambda_0$), because the double wire medium can be characterized by a very large positive index of refraction with anomalous frequency dispersion in the low frequency limit.[21,26] It is interesting to mention that the electromagnetic response of wire media typically has a dual behavior, and so, depending on the excitation, the metamaterial may behave either as an effective medium with positive permittivity or as a material with negative permittivity.[32]

To illustrate the application of the method in case of metallic loss, next we suppose that the metal permittivity $\varepsilon_0\varepsilon_m$ has a Drude-type dispersion so that $\varepsilon_m = 1 - \frac{\omega_p^2}{\omega(\omega+i\Gamma)}$, where ω_p is the plasma frequency and Γ is the collision frequency. It is assumed that the plasma frequency is such that $\omega_p a/c = 0.125$ and that the collision frequency is $\Gamma/\omega_p = 0.05$. The remaining structural parameters, as well as the incoming wave, are as in Fig. 2. The reflection and transmission coefficients calculated with the IDF approach and with the analytical (ABC based) approach[12] are plotted in Fig. 4. As seen, the agreement between the FDFD-SD results and the analytical model is excellent, confirming that the constitutive relation in Eqs. (13a) and (13b) is valid across the interfaces between different media even in a case of metal loss.

Next, we consider a case in which the metamaterial slab is backed by a metallic region (a good conductor, which we refer to as the ground plane; the permittivity of the ground plane is taken as $\varepsilon_h \to -\infty$). The incoming wave propagates in air as in the previous examples, and the angle of incidence is taken as $\theta_i = 70°$. The thickness of the slab is $L = 20a$, the radius of the wires is $r_w = 0.05a$, and the relative permittivity of the host region is $\varepsilon_h = 30$. The metallic wires are assumed to be PEC.

We consider a scenario in which the metallic wires are in ohmic contact with the ground plane. In the DIT2 formalism (see Sec. II B), there is no way of specifying that the metallic wires are in contact with the ground plane. However, in the DIT1 and IDF models, this can be taken into account by imagining that the wires are slightly prolonged into the metal so that they penetrate a thin transition layer inside the metal. Thus, in the transition layer, the parameter β_p (which only depends on the radius of the wires) is taken to be the same as in the metamaterial region. Farther inside the metal, similar to the previous examples, we take the limit $\beta_p \to 0$ to model that the wires are severed past the transition layer. In the numerical implementation, the thickness of the metal transition layer was taken as equal to $0.04L$.

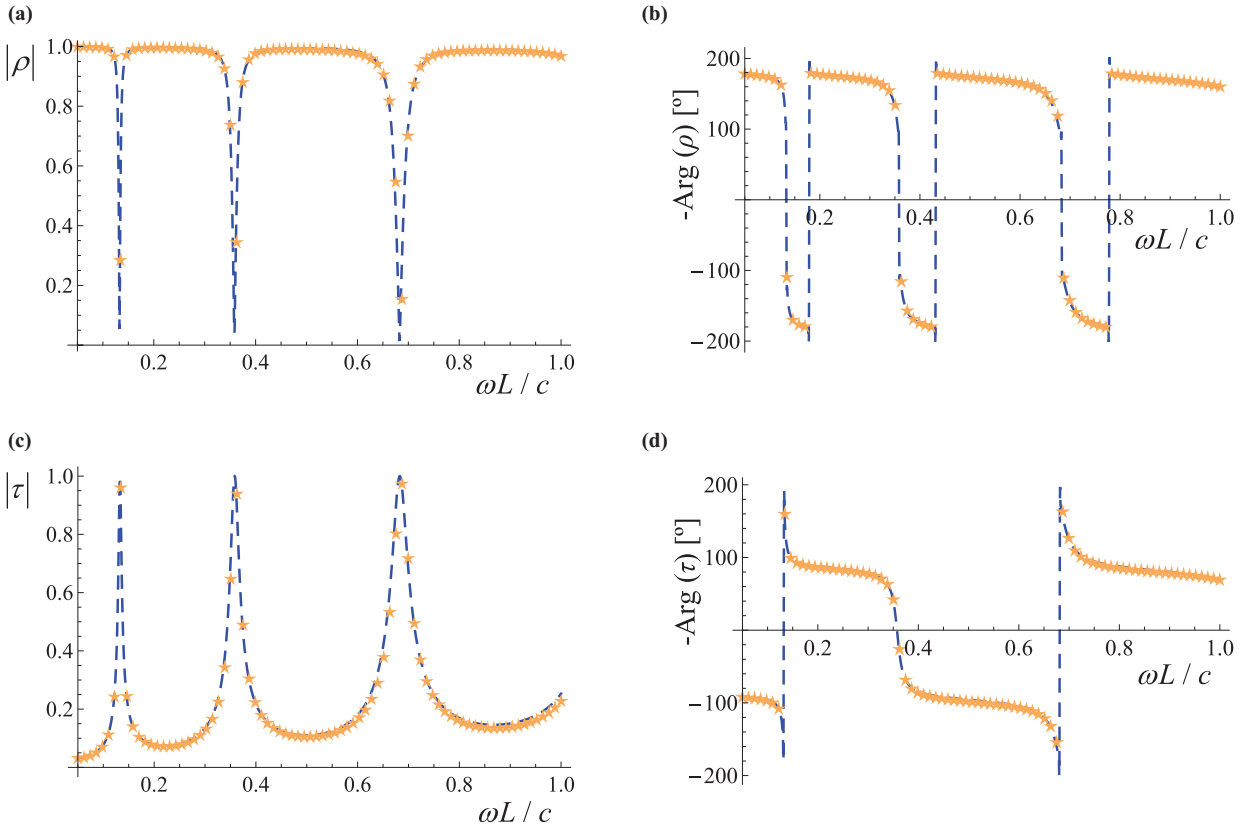

FIG. 3. (Color online) Same example as in Fig. 2. Dashed (blue) curves show full-wave results obtained with CST Microwave Studio (Ref. 33). Stars (orange) indicate the IDF approach (see Sec. III B).

In Fig. 5, we depict the phase of the reflection coefficient ρ as a function of frequency. Similar to the previous examples (Figs. 2 and 4), it is seen in Fig. 5(a) that the agreement between the analytical method based on ABCs (solid black curve) and the IDF approach is nearly perfect. The results also concur well with full-wave simulations that take into account the granularity of the metamaterial (dashed blue curve). However, both the DIT1 and the DIT2 approaches yield wrong results [Fig. 5(b)], because they are unable to capture the dynamics of the current along the wires in the vicinity of the ground plane. This not only confirms that proper discretization is of vital importance at the interfaces, but also shows that the DIT1 and DIT2 methods are inaccurate in a scenario where the double wire medium is attached to a metallic surface.

We underline that the FDFD implementations do not require any ABCs, because they assume that Eq. (9) or Eq. (13a), depending on the implementation, are valid across the interface. In some sense, as already mentioned in Sec. I, in the FDFD implementations the ABCs are indirectly enforced by the adopted form of the constitutive relation across the interface. For example, for the IDF approach, Eq. (13a) implicitly imposes that both $P_{c,z}$ and $\frac{1}{\varepsilon_h \beta_p^2}\frac{\partial P_{c,z}}{\partial x}$, with $P_{c,z} = D_z - \varepsilon_0 \varepsilon_h E_z$, be continuous across the interfaces. In the case of a wire medium adjacent to a dielectric (e.g., air region), this implies (because we take $\beta_p^2 \to 0$ in the dielectric) that $\partial_x P_{c,z}|_{\text{diel}} = 0$ at the dielectric side of the boundary. This homogeneous boundary condition effectively ensures (together with the PML boundary conditions) that $P_{c,z} = 0$ in the dielectric region and thus, because $P_{c,z}$ is continuous at the boundary, that the conduction current vanishes at the wire medium side of the interface, $P_{c,z}|_{WM} = 0$, which is equivalent to the ABC used in Ref. 12. On the other hand, if the wire medium is adjacent to a metal transition layer (such that the wires are prolonged into the metal), the continuity of $\frac{1}{\varepsilon_h \beta_p^2}\frac{\partial P_{c,z}}{\partial x}$ enforces that $\partial_x P_{c,z}|_{WM} = 0$ at the wire medium side of the boundary, because $\varepsilon_h \to -\infty$ at the metal side. This boundary condition is also equivalent to that considered in Ref. 12. Thus, it follows that the IDF approach is compatible with the ABC formalism described in our previous work.[12] On the other hand, the ABCs implicitly enforced by the DIT1 method are the continuity of $P_{c,z}$ and $\partial_x P_{c,z}$ at the interfaces. These in general are inconsistent with the microstructure of the material, because we should have $\partial_x P_{c,z}|_{\text{diel}} = 0$ and $P_{c,z}|_{\text{diel}} = 0$ at the dielectric side of the boundary, rather than the continuity of $P_{c,z}$ and $\partial_x P_{c,z}$.

The geometries considered in all previous examples are quite elementary; therefore, the considered problems admit an analytical solution based on mode matching and ABCs.[12] However, one of the key features of the FDFD-SD approach is that it enables us to obtain the solution of scattering and waveguiding problems in scenarios wherein electromagnetic waves interact with complex arbitrary shapes of spatially dispersive bodies. Typically, such problems cannot be solved using analytical methods.

To illustrate this, in what follows, we investigate the imaging of a source by a metamaterial slab with a finite

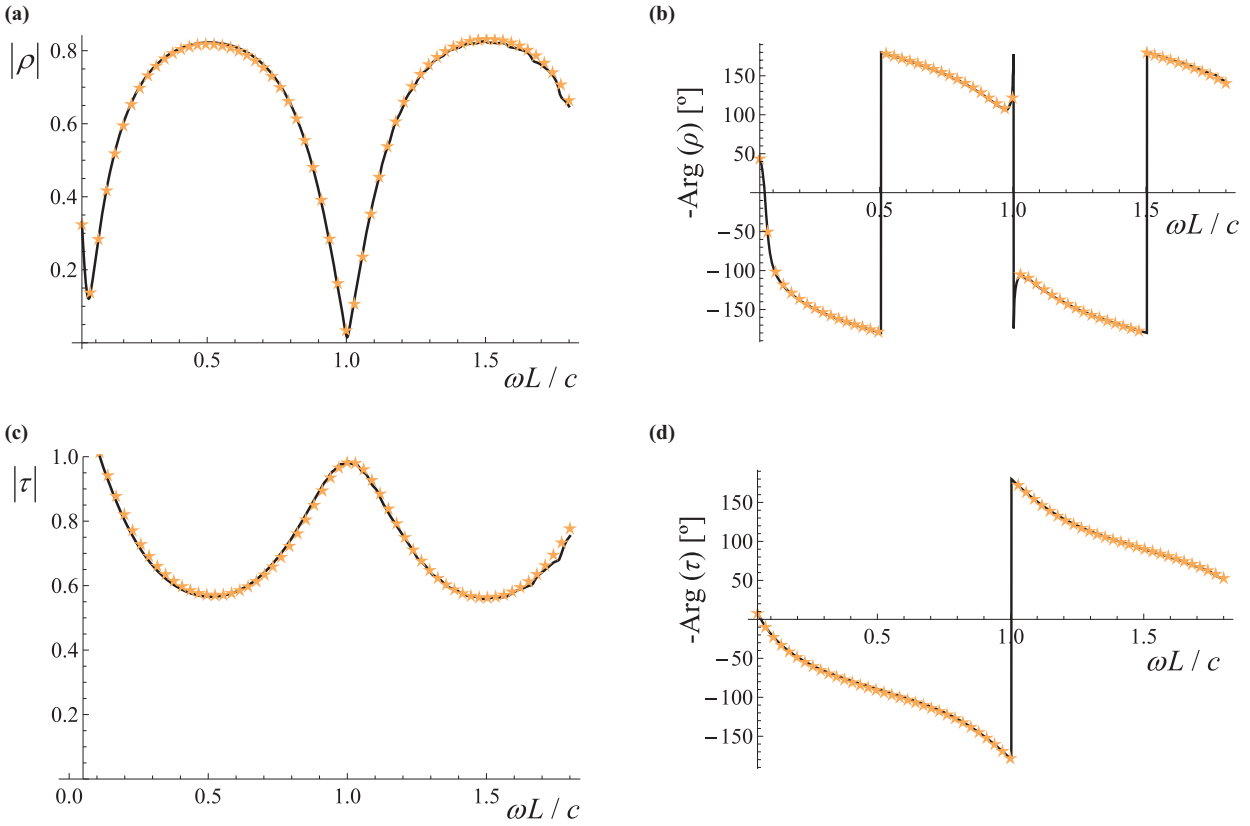

FIG. 4. (Color online) Similar to Fig. 2, but the permittivity of the wires is described by the Drude model $\varepsilon_m = 1 - \omega_p^2/\omega(\omega + i\Gamma)$. The parameters of the Drude model are $\omega_p a/c = 0.125$ and $\Gamma/\omega_p = 0.05$. Solid (black) curves indicate the mode-matching approach based on ABCs (Ref. 12). Stars (orange) indicate the IDF approach (see Sec. III B).

width [inset of Fig. 6(a)]. Previous works[18,19,34] have shown that a high-index dielectric material can be used as a lens that enhances the near field and the subwavelength details, and thus enables a superlensing effect. In Refs. 18 and 19, it was theoretically suggested and experimentally verified that an ultradense array of crossed metallic wires may have a large index of refraction and may support highly confined modes with very short propagation wavelengths, which when excited by a source permit restoration of the subwavelength spatial spectrum. Next, we study the imaging properties of the double wire medium based on the FDFD-SD (IDF) discretization.

We consider a double wire medium with a thickness $L = 10a$ in the near field of an electric line source placed at a distance $d_1 = 0.04\lambda_0$ above the metamaterial [inset of Fig. 6(a)]. The radius of the wires is $r_w = 0.05a$, and

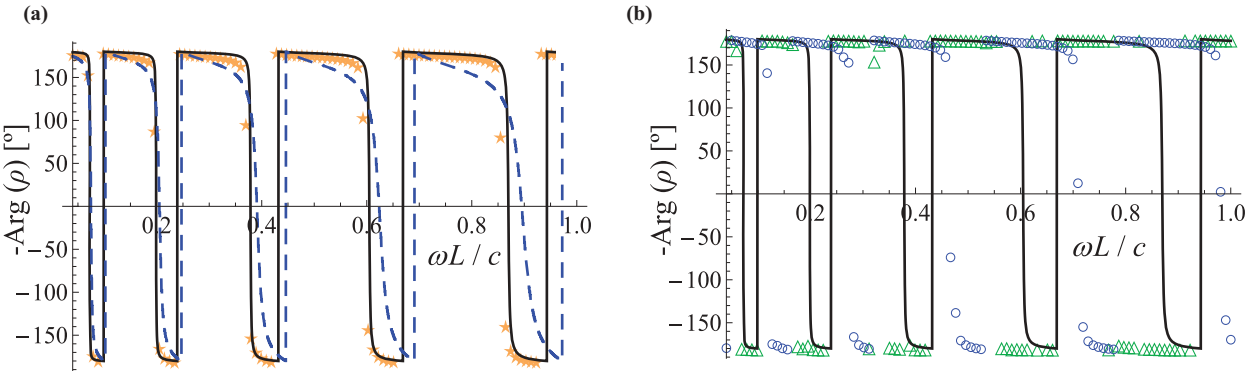

FIG. 5. (Color online) Phase of the reflection coefficient ρ as a function of the normalized frequency for a double wire medium slab with thickness L, backed by a PEC surface. Solid (black) curves indicate the mode-matching approach based on ABCs (Refs. 11 and 12). (a) Stars (orange) indicate the IDF approach (see Sec. III B), and the dashed (blue) curve shows the results obtained with CST Microwave Studio (Ref. 33). (b) Triangles (green) indicate the DIT1 approach, and circles (blue) indicate the DIT2 approach (see Sec. II B).

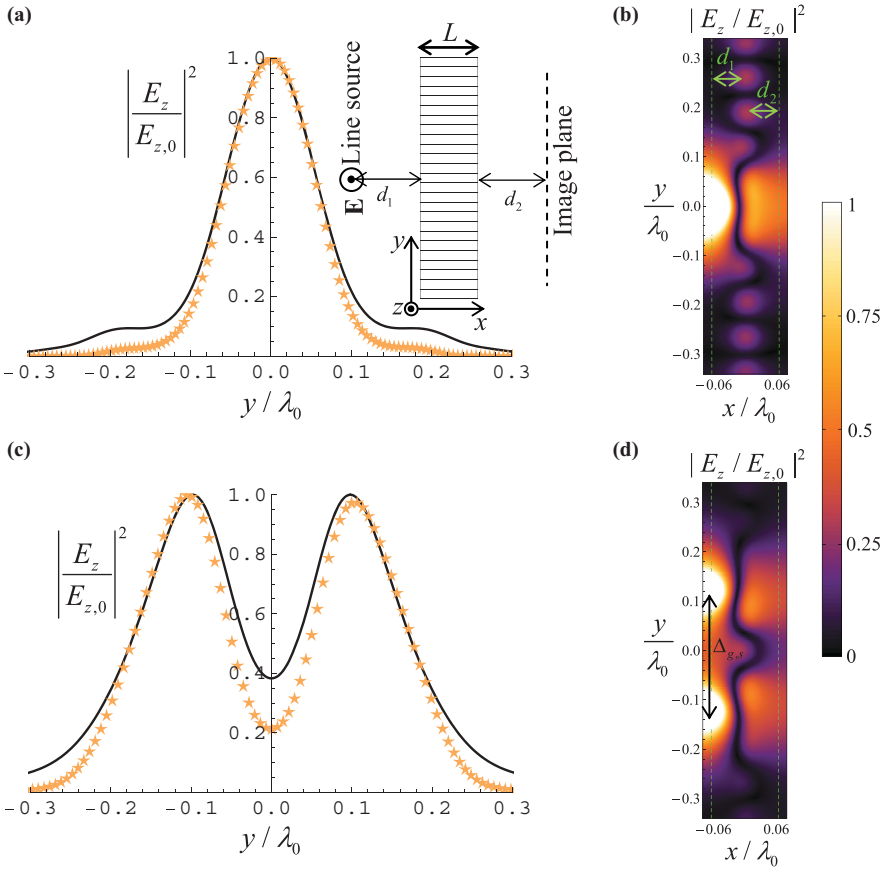

FIG. 6. (Color online) (a) Amplitude of the normalized squared electric field imaged by a metamaterial lens with $L = 0.3\lambda_0/2\pi$, $a = L/10$, and $r_w = 0.05a$ (see the inset). The solid (black) curve indicates the analytical model (Ref. 18). Stars (orange) indicate the FDFD-SD method. (b) Density plot of the normalized electric field for the scenario of panel (a). (c) and (d) are similar to (a) and (b), respectively, but for a case in which the metamaterial lens is illuminated by two electric sources separated by a distance $\Delta_{g,s} = 0.25\lambda_0$.

the normalized frequency of operation is $\omega L/c = 0.3$. It is assumed that the wires are PEC and stand in air. The width of the slab in the y-direction is $w = 1.2\lambda_0$.

Figure 6(a) shows the normalized electric field profile at a distance $d_2 = d_1$ below the lens calculated using the FDFD-SD method (orange stars), and Fig. 6(b) shows the associated electric field density plot. The predicted half-power beamwidth (HPBW) is $0.13\lambda_0$, which is nearly four times smaller than the traditional diffraction limited value. In the absence of the metamaterial lens, and for the same propagation distance $(d_1 + d_2)$ in the air region, the HPBW would be $0.32\lambda_0$, which clearly confirms that the metamaterial lens can restore the subwavelength details of the source and compensate for the evanescent decay in the air regions. We also calculated the electric field profile using an analytical model (black solid curve in Fig. 6(a)) based on a Sommerfeld-type integral (see Ref. 18 for details). The analytical method assumes that the metamaterial slab has an infinite width w in the y-direction. As seen in Fig. 6(a), the results obtained with the analytical model concur well with the FDFD-SD simulations.

In Figs. 6(c) and 6(d), we consider a scenario similar to that of Figs. 6(a) and 6(b), but in this case the metamaterial lens is illuminated by two electric sources separated by a distance $\Delta_{g,s} = 0.25\lambda_0$ [Fig. 6(d)]. It can be seen in Fig. 6(c) that the metamaterial lens clearly discriminates two sources separated by a distance nearly two times inferior to the diffraction limit. The agreement between the analytical results and the FDFD-SD method is again satisfactory.

V. CONCENTRATING THE ELECTROMAGNETIC FIELD WITH A DOUBLE WIRE MEDIUM WAVEGUIDE

It is known that by tapering plasmonic waveguides, one can slow and ultimately stop light[35–37] and concentrate electromagnetic energy in the nanoscale.[35,38] In what follows, we show that by tapering a double wire medium waveguide, it is possible to enhance significantly the magnetic field toward the tip of the waveguide.

First, we use the FDFD-SD (IDF) method to characterize the guided modes supported by an ultradense array of metallic wires.[21] Figure 7(a) shows the dispersion characteristic of the transverse electric (TE) surface wave modes supported by a dense array of PEC wires for different lattice constants a. The discrete orange stars were calculated using the FDFD-SD method, and the black solid curves were obtained using an analytical method based on mode matching and ABCs.[21]

Dispersion of the guided modes is determined with the FDFD-SD method as follows: For each wavelength of operation (λ_0), the metamaterial slab is excited by an electric line source placed within the waveguide. Then, the guided wavelength λ_g is determined by inspection of the real part of the electric field along the central line of the metamaterial slab (i.e., in the direction of propagation) at a distance sufficiently large ($\sim 0.2\lambda_0$) from the source. The effective index of refraction seen by the guided mode is $n_{\text{eff}} = \lambda_0/\lambda_g = k_y c/\omega$.

Consistent with Ref. 21, Fig. 7(a), shows that the metamaterial supports extremely subwavelength guided modes characterized by a large effective index of refraction

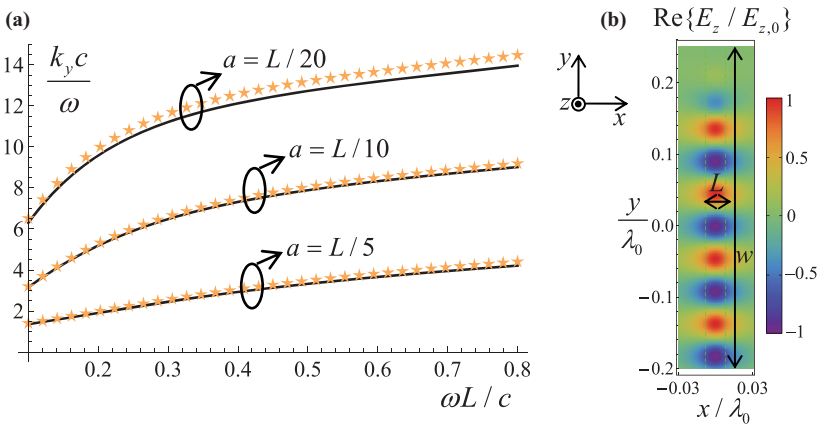

FIG. 7. (Color online) (a) Normalized propagation constant k_y of the TE-guided modes as a function of frequency for a fixed thickness L of the metamaterial formed by PEC wires and different lattice constants a. The radius of the wires is $r_w = 0.05a$, and the wires stand in air. The solid (black) curve indicates the analytical model (Ref. 21). Stars (orange) indicate the FDFD-SD method. (b) Time snapshot of E_z (in arbitrary unities) at the frequency $\omega L/c = 0.1$ when a waveguide with $a = L/20$ is excited by an electric line source positioned at $(0, -0.2\lambda_0)$.

$n_{\mathrm{eff}} = k_y c/\omega$. Moreover, the index of refraction of a guided mode increases as the lattice constant a decreases, i.e., as the density of wires increases for a fixed metal volume fraction. Agreement between the results predicted by the numerical method and those predicted by the analytical model of Ref. 21 is excellent. Figure 7(b) shows a snapshot in time of the electric field in the xoy plane for a double wire medium waveguide with lattice constant $a = L/20$ at the normalized frequency of operation $\omega L/c = 0.1$. As seen, the guided mode is strongly confined to the waveguide, in agreement with the effective index of refraction being $n_{\mathrm{eff}} = 6$ [Fig. 7(a)].

How can this waveguide be tapered so that the guided electromagnetic energy can be concentrated in an ultra-subwavelength region? To answer this question, first we consider two cascaded waveguides with thicknesses L and L_2 [Fig. 8(a)]. We want to obtain a matching condition for two waveguides so that we can ensure a good transmission at the junction. To this end, a transmission line analogy is considered so that each waveguide is associated with a voltage V_i, a current I_i, and an impedance Z_i $(i = 1,2)$. To a first approximation, the field component H_y is proportional to the microscopic current flowing in the metallic wires; thus, it should vanish at the interfaces. Therefore, from the point of view of the waves inside the waveguide, the interfaces with air may be regarded as magnetic walls (perfect magnetic conductor, or PMC). Hence, the guided mode is expected to be quasitransverse electromagnetic (quasi-TEM) with respect to the direction of propagation (y-direction), and the relevant field components are E_z and H_x. Moreover, we can establish the following correspondences:

$$V \sim H_x L, \tag{15a}$$

$$I \sim E_z, \tag{15b}$$

$$Z \sim \frac{H_x}{E_z} L, \tag{15c}$$

where L is the thickness of the metamaterial slab in the x-direction. V was associated with H_x and I with E_z, because a waveguide with PMC walls is the electromagnetic dual of a standard waveguide with PEC walls. On the other hand, for a TE mode, $H_x \sim \frac{\partial E_z}{\partial y}$, and hence the fields inside the waveguide also satisfy

$$\frac{H_x}{E_z} \sim k_y. \tag{16}$$

From Eqs. (15c) and (16), it follows that to keep the impedance constant in the two waveguides and thus ensure a good matching at the transition, one should guarantee that

$$k_y L = \text{const.} \tag{17}$$

Figure 8(a) shows a density plot of the normalized electric field for a metamaterial waveguide similar to that of Fig. 7(a) $(a = L/20)$ in cascade with another waveguide with the thickness $L_2 = 0.6L$. The frequency of operation is $\omega L/c = 0.25$. The lattice constant a_2 of the second waveguide is determined so that Eq. (17) is satisfied, i.e., that $k_y L = k_{y,2} L_2$, where k_y and $k_{y,2}$ represent the wave numbers in the waveguide with thicknesses L and L_2, respectively. This can be done using the analytical model of Ref. 21, provided $k_{y,2}$ and

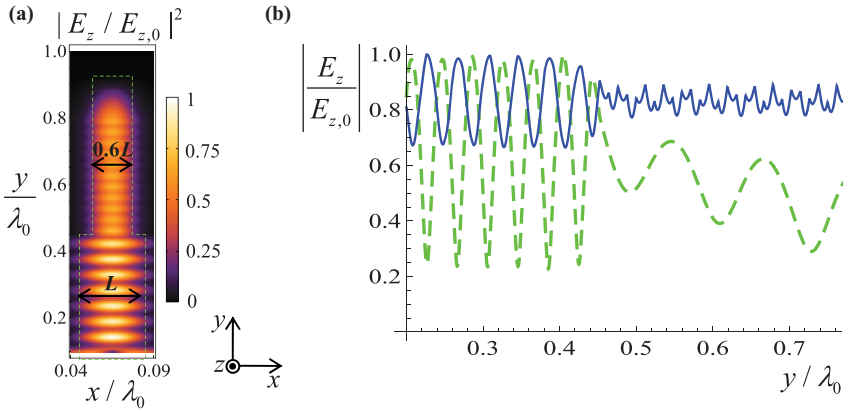

FIG. 8. (Color online) (a) Normalized $|E_z|^2$ in the vicinity of two cascaded double wire medium waveguides with thicknesses L and $L_2 = 0.6L$ at the frequency of operation $\omega L/c = 0.25$. The fields were obtained using the FDFD-SD full-wave simulator. (b) Profile of the square normalized electric field along the central line of the waveguide. Solid (blue) curve: lattice constant in the second waveguide region is tuned so that the impedance matching condition Eq. (17) is satisfied. Dashed (green) curve: lattice constant in the second waveguide region is tuned so that $k_y = k_{y,2}$.

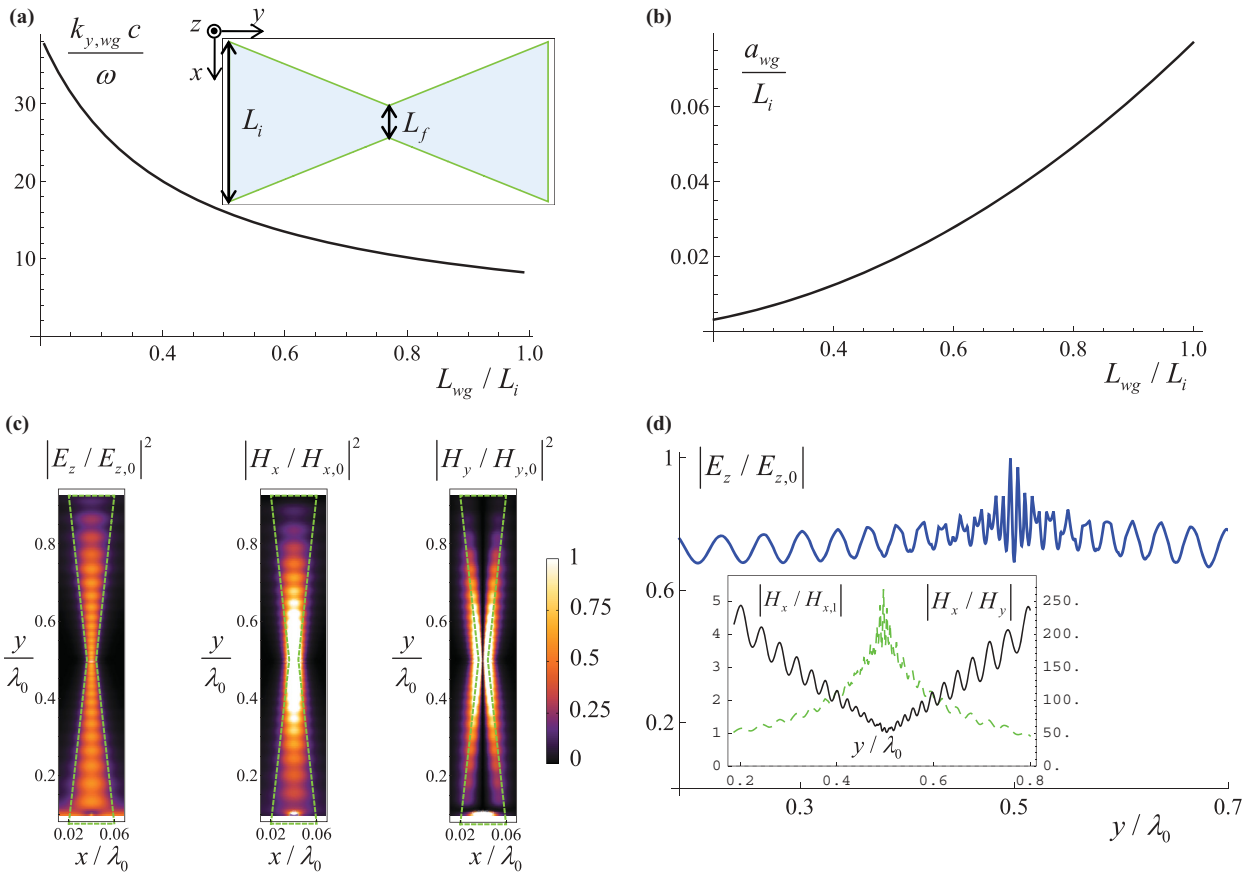

FIG. 9. (Color online) (a) The y-component of the guided wave number $k_{y,wg}$ [calculated using Eq. (17)] as a function of the normalized thickness of the tapered metamaterial waveguide. The geometry of the waveguide is shown in the inset. (b) Normalized lattice constant a_{wg} as a function of the thickness of the waveguide. (c) Normalized $|E_z|^2$, $|H_x|^2$, and $|H_y|^2$ in the vicinity of the tapered waveguide. (d) Profile of the normalized electric field along the central line of the waveguide. The inset shows the profile of H_x/H_y along the central line of the waveguide (solid black curve) and H_x normalized to the amplitude of the x-component of the magnetic field in a waveguide with the constant thickness $L = L_i$.

L_2 are known. The density plot of Fig. 8(a) shows that the electric field amplitude is kept nearly constant across the junction of the two waveguides, indicating good matching. This result is confirmed in Fig. 8(b), where the profile of the normalized electric field along the central line of the waveguide is depicted (solid blue curve). It can be seen that despite the abrupt transition, the wave is barely reflected. In contrast, the green dashed curve is obtained without ensuring the impedance match (specifically, the lattice constant a_2 is tuned so that $k_y = k_{y,2}$); in this case, a standing wave pattern with a much stronger modulation is obtained.

Next, we apply this theory to investigate waveguiding by a tapered metamaterial slab formed by PEC wires with the initial thickness L_i, that is first tapered toward a tip with thickness $L_f = 0.2L_i$ and then expanded toward its original thickness L_i [inset of Fig. 9(a)]. The taper profile is linear and the distance between the points with thickness L_i and L_f is $0.45\lambda_0$. We define $L_{wg} \equiv L_{wg}(y)$ as the thickness of the waveguide as a function of position. The frequency of operation is $\omega L_i/c = 0.25$, and the lattice constant at the beginning of the waveguide is $a_i = L_i/13$.

Figure 9(a) shows the effective index of refraction $n_{wg} \equiv k_{y,wg}c/\omega$ seen by the guided mode toward the tip of the waveguide, where $k_{y,wg} \equiv k_{y,wg}(L_{wg})$ is the wave number in the y-direction determined so that Eq. (17) is satisfied for each L_{wg}. As expected, n_{wg} increases significantly as the tip is approached. In Fig. 9(b), we depict the required lattice constant a_{wg} as a function of the thickness of the waveguide. Figure 9(c) shows a density plot of the normalized electromagnetic fields along the waveguide. Consistent with the results reported in Fig. 8, the electric field remains essentially constant along the waveguide, despite the tapering. This is supported by Fig. 9(d), which shows the normalized electric field profile (blue solid curve) along the axis of the waveguide. The ripple observed in the electric field profile in the vicinity of the tip may be related to numerical imprecision, because near the tip the guided wavelength is extremely small; thus, a refined mesh is required to obtain fully converged results. In contrast, both components of the magnetic field are strongly enhanced as the tip is approached, indicating that tapering the metamaterial waveguide permits concentration of the magnetic field into a subwavelength spot [Fig. 9(c)]. This also shown in the inset of Fig. 9(d), which depicts H_x/H_y (black solid curve) and $H_x/H_{x,1}$ (green dashed curve) along the axis of the waveguide, where $H_{x,1}$ is the amplitude of the x-component of the magnetic field in a waveguide with the constant thickness $L = L_i$. It is evident that H_y is nearly negligible compared to H_x (black solid curve), indicating that

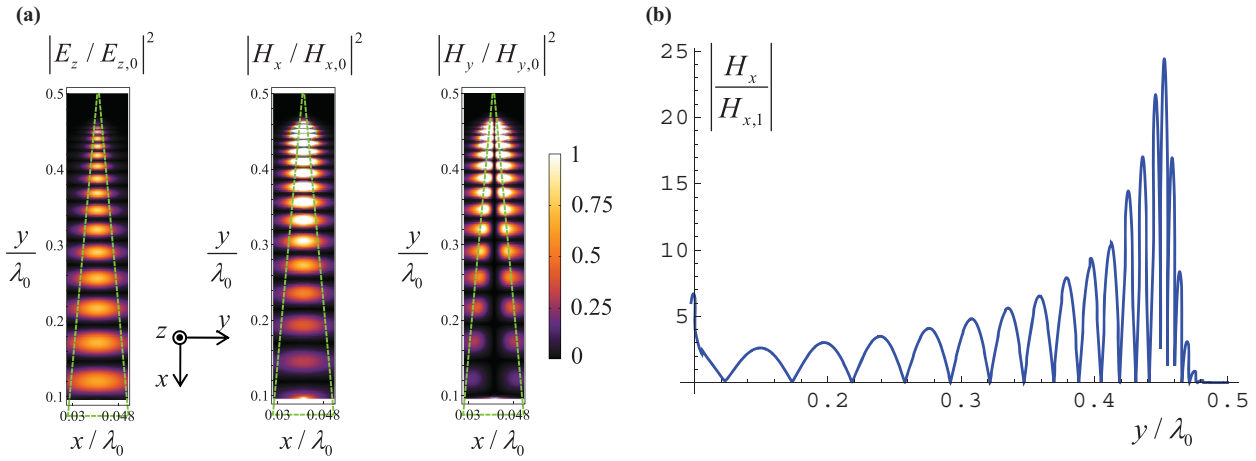

FIG. 10. (Color online) (a) Normalized $|E_z|^2$, $|H_x|^2$, and $|H_y|^2$ in the vicinity of a tapered double wire medium waveguide, with initial and final thicknesses $L_i = 15a_i$ and $L_f = 0.03L_i$, respectively. The frequency of operation is $\omega L_i/c = 0.15$. (b) Profile of the magnetic field along the central line of the waveguide. H_x is normalized to the amplitude of the x-component of the magnetic field in a waveguide with the constant thickness $L = L_i$.

we indeed have quasi-TEM propagation, in agreement with our initial assumption. Moreover, H_x is enhanced about five times with respect to a waveguide with the constant thickness $L = L_i$ (green dashed curve), which is consistent with $L_f/L_i = 5$.

We also studied a case where the waveguide is tapered and severed at the tip. In this example, the parameters of the waveguide are $a_i = L_i/15$ and $L_f = 0.03L_i$ and the frequency of operation is $\omega L_i/c = 0.15$. Figure 10(a) shows a density plot of the normalized electromagnetic fields in the vicinity of the tapered waveguide. The results are consistent with the previous example, because the electric field is nearly constant along the waveguide and both components of the magnetic field are greatly enhanced. Figure 10(b) represents the x-component of the magnetic field along the axis of the waveguide. In agreement with the results of Fig. 9(d), the enhancement of the magnetic field is roughly inversely proportional to the compression of the waveguide, confirming that this is an exciting possibility to enhance the magnetic fields in an ultra-subwavelength region.

VI. CONCLUSIONS

It was argued that knowledge of the bulk electromagnetic response of a spatially dispersive material is insufficient to characterize the response to a macroscopic external excitation in the presence of interfaces, even in simple scenarios where the geometry of the interfaces is trivial. The partial differential equations that link **D** and **E**, obtained by inverse Fourier transforming the constitutive relations in the spectral domain, may not hold across a boundary between two materials. Moreover, it is possible to link **D** and **E** through inequivalent differential equations over the interfaces, even though they are consistent in the bulk regions. The correct form of the differential equations across the boundary can only be determined based on knowledge of the internal structure of the metamaterial. It was illustrated how this can be done in practice for the particular case of a double wire medium, and a general FDFD-SD approach was developed to accurately characterize the electromagnetic response of spatially dispersive wire medium bodies with arbitrary geometries. As an application of the developed methods, we investigated the possibility of concentrating the electromagnetic fields at the tip of an ultracompact tapered waveguide formed by wire media, showing that this may be an exciting route for enhancing and focusing the magnetic field in a subwavelength spot.

ACKNOWLEDGMENTS

This work was partially supported by Fundação para Ciência e a Tecnologia under Project No. PTDC/EEATEL/100245/2008. J.T.C. acknowledges financial support by IT and Fundação para a Ciência e a Tecnologia under Fellowship No. SFRH/BD/36976/2007.

APPENDIX A

In this Appendix, it is shown that the differential system in Eq. (12) can be written exclusively in terms of the electromagnetic fields E_z, D_z, H_x, and H_y.

First, from the theory of Refs. 13 and 27, the macroscopic response of the wire medium can be described by [this set of equations is represented in a compact manner by Eq. (12)]:

$$\nabla \times \mathbf{E} = i\omega\mu_0 \mathrm{H} \tag{A1}$$

$$\nabla \times \mathbf{H} = \mathbf{j}_{\mathrm{ext}} - i\omega\mathbf{D} \tag{A2}$$

$$\frac{\partial}{\partial x_\alpha}\varphi_\alpha = -(Z_w - i\omega L_w)I_\alpha + E_\alpha \tag{A3}$$

$$\frac{\partial}{\partial x_\alpha} I_\alpha = i\omega C_w \varphi_\alpha \tag{A4}$$

$$\mathbf{D} = \varepsilon_0\varepsilon_h\mathbf{E} + \frac{1}{-i\omega}\sum_\alpha \frac{I_\alpha}{A_{\mathrm{cell}}}\hat{\mathbf{u}}_\alpha \tag{A5}$$

Here, $A_{\mathrm{cell}} = a^2$, $\hat{\mathbf{u}}_\alpha$ is a unit vector that defines the orientation of the αth set of wires ($\alpha = 1,2$); C_w, L_w, and Z_w are the effective capacitance, inductance, and self-impedance of

the wires per unit length of a wire, respectively;[13,27] $\mathbf{j}_{\rm ext}$ represents an external excitation; and the second term on the right-hand side of Eq. (A5) is the macroscopic density of current associated with flow of charges along the metallic wires, $\mathbf{J}_w = \sum_\alpha \frac{I_\alpha}{A_{\rm cell}}\hat{\mathbf{u}}_\alpha$. In the above, I_α and φ_α are the current and additional potential, respectively, associated with the αth set of wires, and $E_\alpha = \hat{\mathbf{u}}_\alpha \cdot \mathbf{E}\ x_\alpha = \hat{\mathbf{u}}_\alpha \cdot \mathbf{r}$, with $\mathbf{r} = (x,y,z)$. Thus, substituting Eq. (A3) into Eq. (A4), we find that

$$C_w \frac{\partial}{\partial x_\alpha}\left(\frac{1}{C_w}\frac{\partial I_\alpha}{\partial x_\alpha}\right) + \left(\frac{\omega}{c}\right)^2 \varepsilon_h I_\alpha + i\omega C_w Z_w I_\alpha = i\omega C_w E_\alpha, \tag{A6}$$

where we used $C_w L_w = \varepsilon_0\varepsilon_h\mu_0$, which holds for the case of straight wires.[27] For the configuration of interest in this work, we know that both the electric displacement vector and the electric field only have a z-component. Therefore, for propagation in the xoy plane, we may write

$$E_\alpha = \mathbf{E}\cdot\hat{\mathbf{u}}_\alpha = E_z\hat{\mathbf{z}}\cdot\hat{\mathbf{u}}_\alpha = E_z\frac{1}{\sqrt{2}} (\alpha = 1,2) \tag{A7}$$

$$\frac{I_\alpha}{A_{\rm cell}} = \mathbf{J}_w\cdot\hat{\mathbf{u}}_\alpha = J_{w,z}\hat{\mathbf{z}}\cdot\hat{\mathbf{u}}_\alpha = J_{w,z}\frac{1}{\sqrt{2}}\ (\alpha = 1,2), \tag{A8}$$

and by substituting Eqs. (A7) and (A8) into Eq. (A6), we obtain

$$C_w \frac{\partial}{\partial x_\alpha}\left(\frac{1}{C_w}\frac{\partial J_{w,z}}{\partial x_\alpha}\right) + \left(\frac{\omega}{c}\right)^2 \varepsilon_h J_{w,z} + i\omega C_w Z_w J_{w,z} = \frac{1}{A_{\rm cell}} i\omega C_w E_z. \tag{A9}$$

On the other hand, $\frac{\partial}{\partial x_\alpha} = \hat{\mathbf{u}}_\alpha\cdot\nabla$, and because we assume $\frac{\partial}{\partial z} = 0$, this implies that $\frac{\partial}{\partial x_\alpha} = \pm\frac{1}{\sqrt{2}}\frac{\partial}{\partial x}$. Hence, we finally obtain the result:

$$\frac{1}{2}C_w\frac{\partial}{\partial x}\left(\frac{1}{C_w}\frac{\partial J_{w,z}}{\partial x}\right) + \left(\frac{\omega}{c}\right)^2 \varepsilon_h J_{w,z} + i\omega C_w Z_w J_{w,z} = \frac{1}{A_{\rm cell}} i\omega C_w E_z \tag{A10}$$

Using Eq. (A5) and the definition of $\mathbf{J}_w$, it follows that $D_z = \varepsilon_0\varepsilon_h E_z - \frac{J_{w,z}}{i\omega}$; hence:

$$\frac{C_w}{2}\frac{\partial}{\partial x}\left[\frac{1}{C_w}\frac{\partial}{\partial x}\left(\varepsilon_h E_z - \frac{D_z}{\varepsilon_0}\right)\right] + \varepsilon_h\left(\frac{\omega}{c}\right)^2\left(\varepsilon_h E_z - \frac{D_z}{\varepsilon_0}\right) + i\omega C_w Z_w\left(\varepsilon_h E_z - \frac{D_z}{\varepsilon_0}\right) = \frac{C_w}{A_{\rm cell}\varepsilon_0}E_z \tag{A11}$$

Finally, we use $\beta_p^2 = \frac{C_w}{\varepsilon_0\varepsilon_h A_{\rm cell}}$ and $Z_w = -\frac{1}{i\omega\pi r_w^2\varepsilon_0\varepsilon_h(\varepsilon_m/\varepsilon_h - 1)} = \frac{\beta_c^2}{i\omega C_w}$, where $\beta_c^2 = -\frac{\beta_p^2}{(\varepsilon_m/\varepsilon_h - 1)f_V}$,[13,27] to rewrite Eq. (A11) as in Eq. (13a) of the main text. On the other hand, Eq. (13b) follows directly from Eqs. (A1) and (A2).

APPENDIX B

Here, we provide explicit formulas for the discretized system in Eqs. (13a) and (13b):

$$\begin{aligned}
&\frac{\varepsilon_h(i,j)\beta_p^2(i,j)}{2}\left[\frac{\varepsilon_h^{-1}(i,j)\beta_p^{-2}(i,j) + \varepsilon_h^{-1}(i+1,j)\beta_p^{-2}(i+1,j)}{2\Delta x^2}P_{c,z}(i+1,j)\right.\\
&-\frac{2\varepsilon_h^{-1}(i,j)\beta_p^{-2}(i,j) + \varepsilon_h^{-1}(i+1,j)\beta_p^{-2}(i+1,j) + \varepsilon_h^{-1}(i-1,j)\beta_p^{-2}(i-1,j)}{2\Delta x^2}P_{c,z}(i,j)\\
&\left.+\frac{\varepsilon_h^{-1}(i,j)\beta_p^{-2}(i,j) + \varepsilon_h^{-1}(i-1,j)\beta_p^{-2}(i-1,j)}{2\Delta x^2}P_{c,z}(i-1,j)\right] + \left[\varepsilon_h(i,j)\left(\frac{\omega}{c}\right)^2 + \beta_c^2(i,j)\right]P_{c,z}(i,j)\\
&+\varepsilon_0\varepsilon_h(i,j)\beta_p^2(i,j)E_z(i,j) = 0
\end{aligned} \tag{B1}$$

$$\frac{E_z(i+1,j) - 2E_z(i,j) + E_z(i-1,j)}{\Delta x^2} + \frac{E_z(i,j+1) - 2E_z(i,j) + E_z(i,j-1)}{\Delta y^2} + \left(\frac{\omega}{c}\right)^2\frac{D_z(i,j)}{\varepsilon_0} = -i\omega\mu_0 j_{s,z}(i,j) \tag{B2}$$

*mario.silveirinha@co.it.pt

[1] V. Agranovich and V. Ginzburg, *Spatial Dispersion in Crystal Optics and the Theory of Excitons* (Taylor Wiley-Interscience, New York, 1966).

[2] Y. Zhao, P. A. Belov, and Y. Hao, Opt. Express **14**, 5154 (2006).

[3] Y. Zhao, P. A. Belov, and Y. Hao, IEEE Trans. Antenn. Propag. **55**, 1506 (2007).

[4] Y. Zhao, P. A. Belov, and Y. Hao, J. Opt. A Pure Appl. Opt. **11**, 075101 (2009).

[5] S. Raza, G. Toscano, A.-P. Jauho, M. Wubs, and N. A. Mortensen, Phys. Rev. B **84**, 121412(R) (2011).

[6] G. Toscano, S. Raza, A.-P. Jauho, N. A. Mortensen, and M. Wubs, Opt. Express **20**, 4176 (2012).

[7] J. M. McMahon, S. K. Gray, and G. C. Schatz, Phys. Rev. Lett. **103**, 097403 (2009).

[8] J. M. McMahon, S. K. Gray, and G. C. Schatz, Phys. Rev. B **82**, 035423 (2010).

[9] F. J. G. de Abajo, J. Phys. Chem. C **112**, 17983 (2008).

[10] C. David and F. J. G. de Abajo, J. Phys. Chem. C **115**, 19470 (2011).

[11] M. G. Silveirinha, C. A. Fernandes, and J. R. Costa, New J. Phys. **10**, 053011 (2008).

[12] M. G. Silveirinha, New J. Phys. **11**, 113016 (2009).

[13] S. I. Maslovski, T. A. Morgado, M. G. Silveirinha, C. S. R. Kaipa, and A. B. Yakovlev, New J. Phys. **12**, 113047 (2010).

[14]P. A. Belov, R. Marqués, S. I. Maslovski, I. S. Nefedov, M. G. Silveirinha, C. R. Simovski, and S. A. Tretyakov, Phys. Rev. B **67**, 113103 (2003).
[15]G. Shvets, A. K. Sarychev, and V. M. Shalaev, Proc. SPIE **5218**, 156 (2003).
[16]C. R. Simovski and P. A. Belov, Phys. Rev. E **70**, 046616 (2004).
[17]M. G. Silveirinha, IEEE Trans. Antenn. Propag. **56**, 390 (2008).
[18]M. G. Silveirinha, C. A. Fernandes, and J. R. Costa, Phys. Rev. B **78**, 195121 (2008).
[19]M. G. Silveirinha, C. R. Medeiros, C. A. Fernandes, and J. R. Costa, Phys. Rev. B **81**, 033101 (2010).
[20]R. A. Shelby, D. R. Smith, and S. Schultz, Science **292**, 77 (2001).
[21]M. G. Silveirinha and C. A. Fernandes, Phys. Rev. B **78**, 033108 (2008).
[22]J. Yao, Z. Liu, Y. Liu, Y. Wang, C. Sun, G. Bartal, A. M. Stacy, and X. Zhang, Science **321**, 930 (2008).
[23]Y. Liu, G. Bartal, and X. Zhang, Opt. Express **16**, 15439 (2008).
[24]G. Shvets, S. Trendafilov, J. B. Pendry, and A. Sarychev, Phys. Rev. Lett. **99**, 053903 (2007).
[25]T. A. Morgado, J. S. Marcos, M. G. Silveirinha, and S. I. Maslovski, Phys. Rev. Lett. **107**, 063903 (2011).
[26]M. G. Silveirinha, Phys. Rev. Lett. **102**, 193903 (2009).
[27]S. I. Maslovski and M. G. Silveirinha, Phys. Rev. B **80**, 245101 (2009).
[28]M. G. Silveirinha and C. A. Fernandes, IEEE Trans. Microw. Theor. Tech. **53**, 1418 (2005).
[29]K. S. Yee, IEEE Trans. Antenn. Propag. **14**, 302 (1966).
[30]K. Yasumoto, *Electromagnetic Theory and Applications for Photonic Crystals* (Taylor and Francis, New York, 2006).
[31]S. D. Gedney, IEEE Trans. Antenn. Propag. **44**, 1630 (1996).
[32]M. G. Silveirinha and S. I. Maslovski, Phys. Rev. B **85**, 155125 (2012).
[33]CST Microwave Studio Suite™ 2010, http://www.cst.com.
[34]J. Christensen and F. J. G. de Abajo, Phys. Rev. B **82**, 161103(R) (2010).
[35]M. I. Stockman, Phys. Rev. Lett. **93**, 137404 (2004).
[36]M. S. Jang and H. Atwater, Phys. Rev. Lett. **107**, 207401 (2011).
[37]K. L. Tsakmakidis, A. D. Boardman, and O. Hess, Nature (London) **450**, 397 (2007).
[38]S. A. Maier, S. R. Andrews, L. Martín-Moreno, and F. J. García-Vidal, Phys. Rev. Lett. **97**, 176805 (2006).